Experiments on Dynamic Buckling of Shallow Spherical Shells Under Shock Loading

J. S. HUMPHREYS,* R. S. ROTH,† AND J. ZATLERS‡
Avco Corporation, Wilmington, Mass.

A series of experiments in a large shock tube on the dynamic buckling threshold of shallow spherical caps has been performed. Circumferential and radial strains on three circles concentric about the cap axis as well as the maximum normal central deflection have been recorded. A comparison has been made with the deflection predictions of a dynamic nonlinear theory, due to Budiansky and Roth, which assumes symmetric deflections and uniform loading. With the measured pressure pulse, these numerical computations predict a critical buckling level about 10 to 20% higher than that observed. The theory appears to be quite unconservative in predicting the maximum deflection itself at low loads; however at postbuckling levels, it estimates this deflection moderately well.

1. Introduction

THE dynamic response and instability of various types of shell structures are problems that continue to pose formidable difficulties to the analyst and remain of current research interest. Recently, a numerical analytical approach has been developed by Budiansky and Roth[1] for the particular case of a shallow spherical cap deforming symmetrically under an arbitrary time-dependent pressure. The nonlinear response of the shell is computed as a function of time for a series of pressure pulse sizes, showing a rather sharp jump in response amplitude at a particular pulse size. This is identified as "dynamic buckling".

The purpose of the shock-tube experiments reported herein has been to test this analytical method in a situation where the dynamic pressure environment is well controlled and reasonably uniform. A detailed pressure calibration is first made using rigid models to determine the pressure pulse shape, which can then be used in the numerical program to obtain a response prediction. This prediction, and in particular the load level at which "dynamic buckling" occurs, can thus be compared directly to various methods of response measurement in the actual blast tests of flexible models.

This comparison provides greater insight into the applicability and limitations of an analysis of this type (which neglects any imperfections of the shell or nonsymmetry of loading or response) in more complex situations and, therefore, more interesting situations that involve this general kind of loading environment.

II. Experimental Setup and Procedure

The test setup in the 6-ft-diam shock tube is shown in Fig. 1. All spherical shells and the flat calibration plate were rigidly clamped in their respective model holders. To shield the strain gages and associated wiring on the backface of the spherical shells, a guard plate was installed between the model holder and the support frame as shown in Fig. 1. To reduce transmission of vibrations to the test models, rubber pads were inserted between the guard plate and the support frame.

The pressure pulse in each test was generated by the detonation of 175-grain/ft Primacord at the closed end of the shock tube. The explosive was distributed over 20 ft of the compression chamber on expendable cross wires attached to the tube wall. The length of tube to the test section was about 150 ft. During this test series, the following instrumentation was used.

1. Pressure Transducers

All pressure transducers used during this series of tests were of the high-frequency piezo-electric Susquehanna Model ST-2 type, which has a rise time of about 5 μsec. Each transducer was mounted in a 1-in. Teflon grommet to reduce its cross sensitivity. The transducer locations are shown in Fig. 1. Prior to testing each day (and more often if necessary), all pressure transducers were calibrated utilizing a 100-psi 2- to 10-msec rise-time pressure pulse obtained from a solenoid-actuated pressure tank.

2. Displacement Gage

Since the available commercial displacement gages exhibited responses too slow to pick up the central deflection of the shallow spherical shells, a simple penetration device was designed and used throughout the tests. Figure 2 shows the configuration and nominal dimensions of this device.

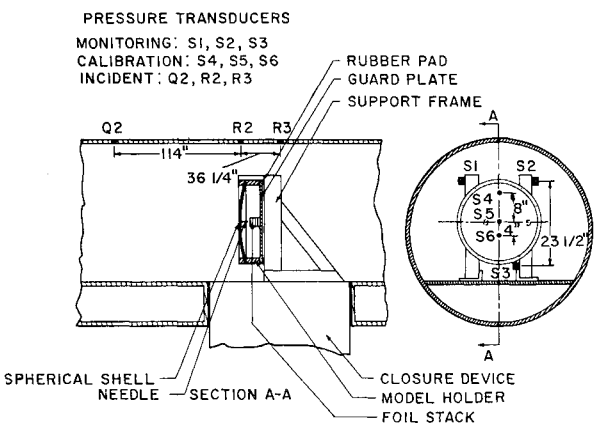

Fig. 1 Shallow spherical shell test setup.

Received February 20, 1964; revision received August 10, 1964. The present test series in a continuing experimental program at the Air Force shock tube facility was conducted under the general supervision of the Air Force Weapons Laboratory, Kirtland Air Force Base, under Air Force Contract No. AFO4(694)-297. The cooperation and interest of the University of New Mexico personnel who operate the shock tube laboratory are gratefully appreciated.

* Senior Staff Scientist, Analytical Mechanics Section, Research and Advanced Development Division. Member AIAA.

† Staff Scientist, Analytical Mechanics Section, Research and Advanced Development Division. Member AIAA.

‡ Test Engineer, Structure Laboratory Section, Research and Advanced Development Division.

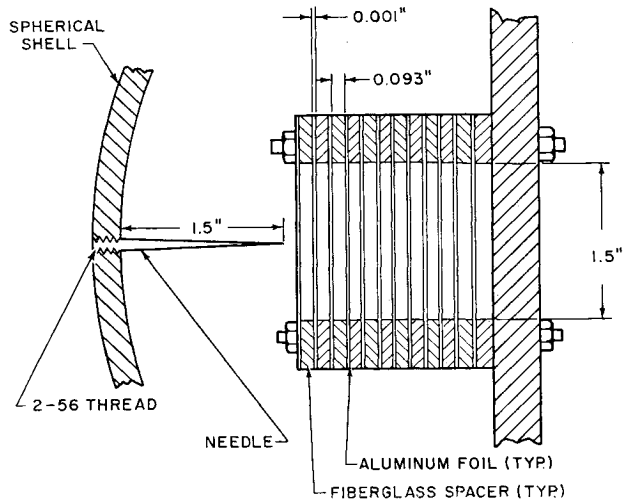

Fig. 2 Penetration device for measurement of maximum central shell deflection.

Upon deflection of the shell, the needle would penetrate a multilayered stack of aluminum foil fastened to the guard plate. After each shot, the stack was examined for total penetration of the needle, and each punctured foil layer was replaced as necessary.

3. Strain Gages

Eighteen Budd C12-121 uniaxial strain gages were attached to the concave surface of each spherical shell to determine qualitatively the presence of dynamic buckling and the symmetry of shell deformation. The strain-gage locations and designation are given in Fig. 3.

4. Readout Equipment

All strain-gage and pressure-transducer outputs were fed into an United Electro-Dynamic data-recording system, which consists of Ampex CP-100 1-in. magnetic-tape recorders with associated switching and timing controls. For all runs, the frequency-modulated method of recording (0- to 20-kc bandwidth), using a carrier frequency of 108 kc, was utilized. For on-the-spot data evaluation, the stored test data were played back and presented on two oscilloscopes where the traces were photographed.

Specific values for the thickness, radius, etc., for each of the four shallow shell models used are given in Fig. 4. Each shell was machined from heavy steel plate. The shells were initially designed to have a geometrical parameter $\lambda = 5$ [where $\lambda^4 = 48\,(1 - \nu^2)H^2/h^2$]; however, because of machining variations, the value of λ actually varied between 4.8 and 4.9. A torque wrench was used to obtain uniform clamping pressure around the edge. Strains observed due to clamping were small (less than 175 μ in./in.).

The general experimental procedure followed was to start at low values of load for a given shell model and progress upward in steps of about 10 to 20 psi (reflected) until a definite dynamic buckling condition was seen, usually accompanied by noticeable permanent plastic set, as determined by measuring the final position of the needle gage.

III. Pressure Calibration

A total of 12 calibration shots were run in the tube using a heavy flat plate in place of the shell model, and with the identical monitoring pressure pickups and support structure as used in the shell tests. Originally, it was planned also to use a curved calibration plate that had been maintained to a shallow spherical curvature; however, the level of variation among the data using the flat plate gave reason to expect that the change in reflected pressures because of the curvature would not be distinguishable.

The reflected pressures from gages S4, S5, and S6 gave a measure of the vertical variation of pressure across the model; it was observed from the data that this variation is not small (up to 20%). This difference appears to be much less when the plate is rotated 90°; i.e., there is little evidence for a horizontal pressure gradient, as may be expected, since the entire setup is symmetrical about a vertical centerline. In both cases, the gage nearest the clamping ring shows a higher peak pressure than the central gage, apparently because of interference from the clamping ring geometry.

In addition to differences in peak pressures, the shape of the whole reflected pulse at the monitoring locations is quite markedly different from the pulse shape at the model location. This is shown in Fig. 5, where traces are compared for a particular test. The main difference in shape is a reduction of the sharp initial spike seen at the model location. The upstream wall pressure, also shown in Fig. 5, shows a

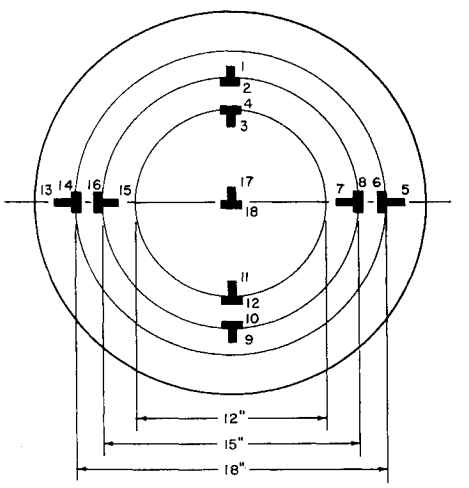

Fig. 3 Strain-gage location on shallow spherical shells (all strain gages: Budd C12-121, gage length $\frac{1}{8}$ in.).

MODEL	TEST	h	H	R (CALC)
1	183-08 TO 189-10	0.195 ± 2 PERCENT	0.701	71.7
2	190-08 TO 191-12	0.200 ± 2 PERCENT	0.687	73.0
3	192-08 TO 192-13	0.161 ± 3 PERCENT	0.562	89.3
4	193-08 TO 193-14	0.161 ± PERCENT	0.564	89.0

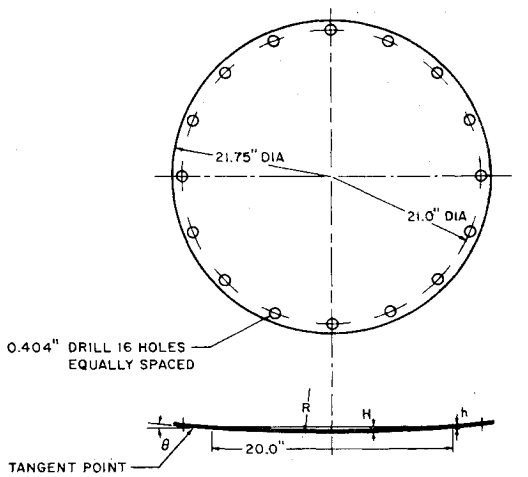

Fig. 4 Shallow spherical cap models.

relatively clean jump across the shock to a slowly decaying overpressure. Based on this overpressure and on the ratio of specific heats for air ($\gamma = 1.4$), one can calculate the theoretical reflected overpressure at a rigid wall from the formula[2]

$$\frac{p_2}{p_1} = \frac{(3\gamma - 1)(p_1/p_0) - \gamma + 1}{(\gamma - 1)(p_1/p_0) + \gamma + 1}$$

where p_0 is ambient pressure and p_1 and p_2 are the incident and reflected shock pressures, respectively. In the particular case of Fig. 5, $p_0 = 15$ psi, $p_1 = 35$ psi and the calculation gives $p_2/p_1 = 2.75$, or $p_2 - p_0 = 123$ psi. This is quite close to the actual peak value of 129 psi observed in Fig. 5a at the center of the model location.

A feature noticeable when the reflected pressure trace is displayed at very high speed is the rather slow rise time of the signal to its peak value (about 50 μsec) compared with what in theory for a shock wave of this type must be an extremely short rise time (1 μsec or less).[2] This must then indicate

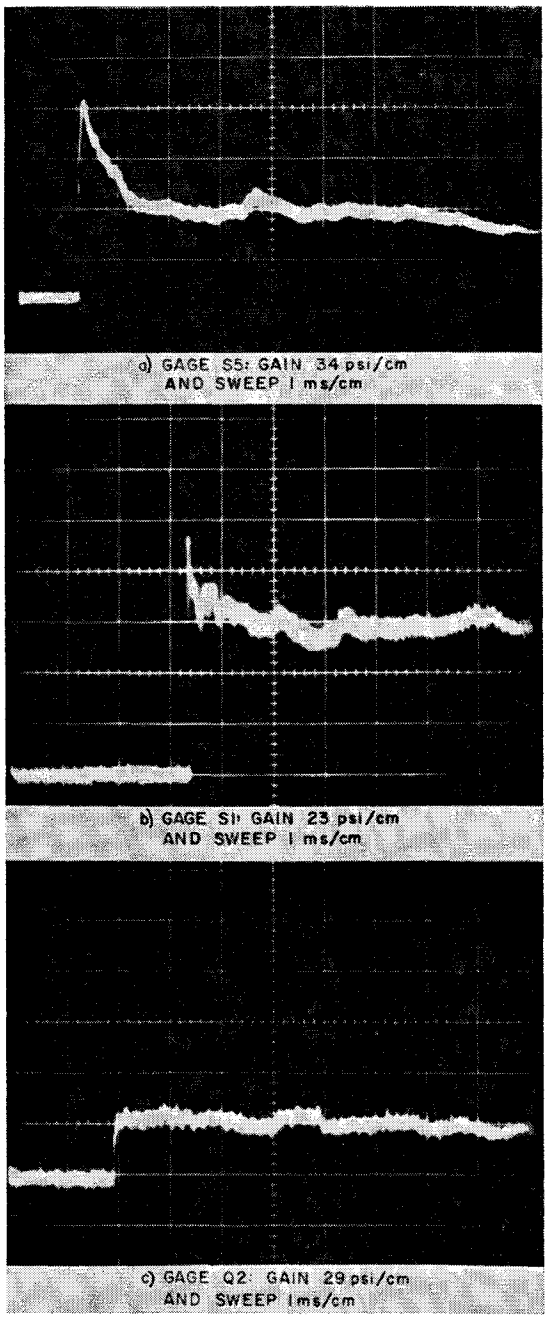

Fig. 5 Comparative pressure response: model center vs monitor location.

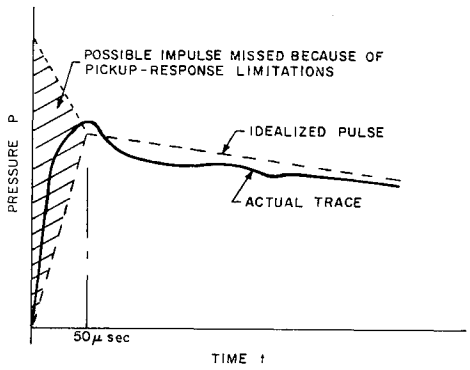

Fig. 6 Initial details of recorded pressure pulse.

a limitation imposed by the frequency response of the existing gage plus cathode-follower circuit. It is significant only in that the pressure behind the shock front is a very rapidly decaying function, and if the pick-up instrumentation lags appreciably behind the input, then a segment of the early peak may be missed, as suggested in Fig. 6, although the forementioned reflection calculation suggests that this is not the case. This point is discussed further in Sec. V.

Various possibilities were tried to obtain the best-possible correlation between monitor-location pressures and model-location pressures. The results are summarized in Fig. 7. An average peak pressure P_{av} over the area of the model was defined, assuming that the actual pressure distribution had a minimum as recorded by the center pickup (S5) and a linear slope upward to the edges varying as determined by the other two pickups (S4 and S6). Calling these pressures P_5, P_4, and P_6, respectively, this average pressure is given by $P_{av} = \frac{1}{12}(5P_4 - 3P_5 - 10P_6)$. These numbers have been plotted in Fig. 7 against corresponding values of various combinations of the peak pressures at the monitoring locations and in each case a smooth curve has been faired through the points. The best correlation seems to be obtained using the average value of all three monitoring pressures (the center curve in Fig. 7), and this is the curve used to obtain P_{av} for the actual shell models. It is not, of course, at all clear how accurately P_{av} represents the real pressure history felt by the deforming shell models. The peak pressures should be very close, but subsequent pressure-time history will presumably be affected to some extent by shell deformations. This is neglected here, for lack of any way of obtaining such data directly, and it is assumed that the same time history and decay times as observed for the calibration plate also can be applied to all of the shell tests.

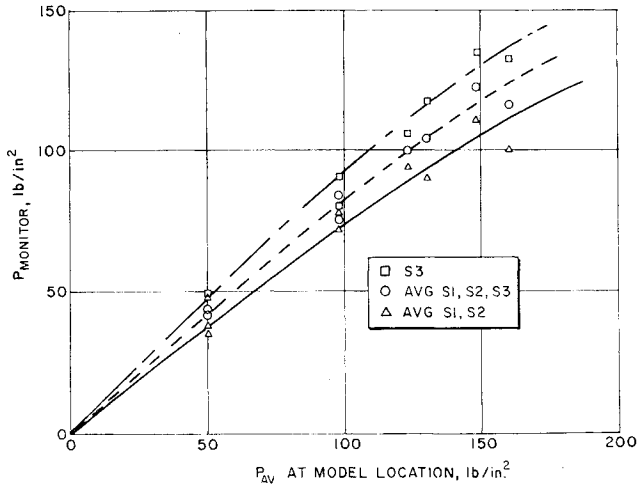

Fig. 7 Correlation of model pressures vs monitor pressures.

IV. Experimental Results

The results of this series of spherical cap tests are summarized in Table 1 and Fig. 8 as far as measured deflections are concerned. The central deformations clearly indicate a sudden rise corresponding to a snapping phenomenon over the range of loading considered. This change, in response with increasing load parameter, is not, however, a clear jump, as in the static buckling situation, nor does it occur in exactly the same way at the same values of nondimensional load parameter for different shells. The load parameter p in each case consists of the peak pressure divided by the critical *static* buckling pressure of a complete sphere of the same thickness and radius under hydrostatic load. The Budiansky-Roth analysis[1] indicates that this is the appropriate load parameter to use for shells with the same geometrical parameter λ.

An essential limitation of this theory is that only symmetric deformation modes were considered. Thus, an important reason for including data on local strains in these tests was to find out whether the buckling deformation proceeded symmetrically. The value of $\lambda = 5$ was chosen originally so that the tests would be located in a region where one would in theory expect the buckling mode to be basically symmetric and the predictions[1] to have some validity. Sample radial strains are shown in Fig. 9 for one of the tests. The recorded strain data confirm the basically symmetric character of the deformations (although gages 7 and 15 differ by 25% in peak value) and also clearly show a snapping phenomenon in which the shell rapidly reaches a rather high value of strain (tensile for the circumferential direction and compressive for the radial direction), and then remains hanging there for about 20 msec before popping back to essentially zero strain.

V. Numerical Calculations

The theoretical problem studied by Budiansky and Roth[1] was to determine the axisymmetric nonlinear response of a clamped, shallow spherical shell subjected to a time-dependent uniform pressure. Because of the shallowness assumption, the initial spherical shape is defined adequately by the parabolic relationship

$$z_0(r) = H[1 - (r/a)^2]$$

and the shell radius R, the base radius a, and the central rise H are related approximately by $a^2 = 2RH$. The problem under consideration is to calculate the time variation of the axisymmetric downward vertical displacement $W(r, t)$ produced by a prescribed history of uniform pressure on the convex surface.

The solution of the governing nonlinear differential equations, taking into account moderately large rotations as well as vertical inertia loads, requires the calculation of the time variation of a finite number of coefficients $a_n (n = 5)$ in the expansion

$$W(r, t) = \sum_n a_n(t)\, W_n(r)$$

wherein the functions $W_n(r)$ are chosen proportional to the natural modes of axisymmetric vibrations of a circular, clamped, flat plate of radius a.

The digital computer solution has been written in terms of the nondimensional geometrical parameter λ (defined previously), a nondimensional time $\tau = ct/R$ [where $c = (E/\rho)^{1/2}$], and a nondimensional pressure parameter $\bar{p} = P_0/q_0$, where

$$q_0 = \frac{2E}{[3(1 - \nu^2)]^{1/2}} \frac{h^2}{R^2}$$

Table 1 Test results for maximum central deflection

Shell	Test	Charge size, ft	Monitor average P, psi	Model average P_{av}, psi	q_0, psi	$\bar{p} = \frac{P_{av}}{q_0}$	Central deformation $W(0)$, in.	$\frac{W(0)}{h}$
1	183-08	78	40	47	267	0.18	0.19	0.98
$h = 0.195$ in.	184-08	78	34	40	267	0.15	0.22	1.2
$R = 71.7$ in.	184-09	150	72	86	267	0.32	0.41	2.1
$H = 0.701$ in.	186-09	150	62	74	267	0.27	0.41	2.1
$\lambda = 4.88$	186-10	225	83	100	267	0.38	1.16	5.9
	189-09	225	(94)[a]	(116)[a]	267	(0.44)	1.35	6.9
2	189-10	300	(92)[a]	(112)[a]	267	(0.42)	1.44	7.4[c]
$h = 0.200$ in.	190-08	78	37	44	272	0.16	$<\frac{1}{8}$	<0.6
$R = 73.0$ in.	190-09	78	34	40	272	0.15	$<\frac{1}{8}$	<0.6
$H = 0.687$ in.	190-10	150	63	75	272	0.28	0.22	1.1
$\lambda = 4.77$	191-08	180	72	86	272	0.32	0.32	1.6
3	191-09	200	78	94	272	0.34	0.34	2.1
$h = 0.161$ in.	191-10	225	110	138	272	0.51	0.57	2.8[b]
$R = 89.3$ in.	191-11	260	121	154	272	0.57	1.10	5.5[b]
$H = 0.562$ in.	191-12	350	145	(202)[a]	272	0.74	1.33	6.7[b, c]
$\lambda = 4.81$	192-10	50	25	29	117	0.24	0.22	1.4
4	192-08	78	35	41	117	0.35	0.32	2.0
$h = 0.161$ in.	192-09	100	48	57	117	0.49	0.60	3.7
$R = 89.0$ in.	192-11	125	69	83	117	0.71	1.01	6.2[b, c]
$H = 0.564$ in.	192-12	150	79	95	117	0.82	1.66	10.3[b, c]
$\lambda = 4.80$	192-13	225	111	139	117	1.19	(1.47)	(9.1)[d]
	193-09	50	28	33	118	0.28	0.10	0.6
	193-10	78	39	46	118	0.39	0.28	1.8
	193-11	100	49	58	118	0.49	0.47	2.9
	193-12	125	59	70	118	0.59	0.92	5.8
	193-13	150	80	97	118	0.83	1.18	7.3[b, c]
	193-14	175	88	107	118	0.91	1.25	7.8[b, c]

[a] Uncertain pressure.
[b] Some permanent set observed.
Snapthrough observed.
[d] Permanent snapthrough.

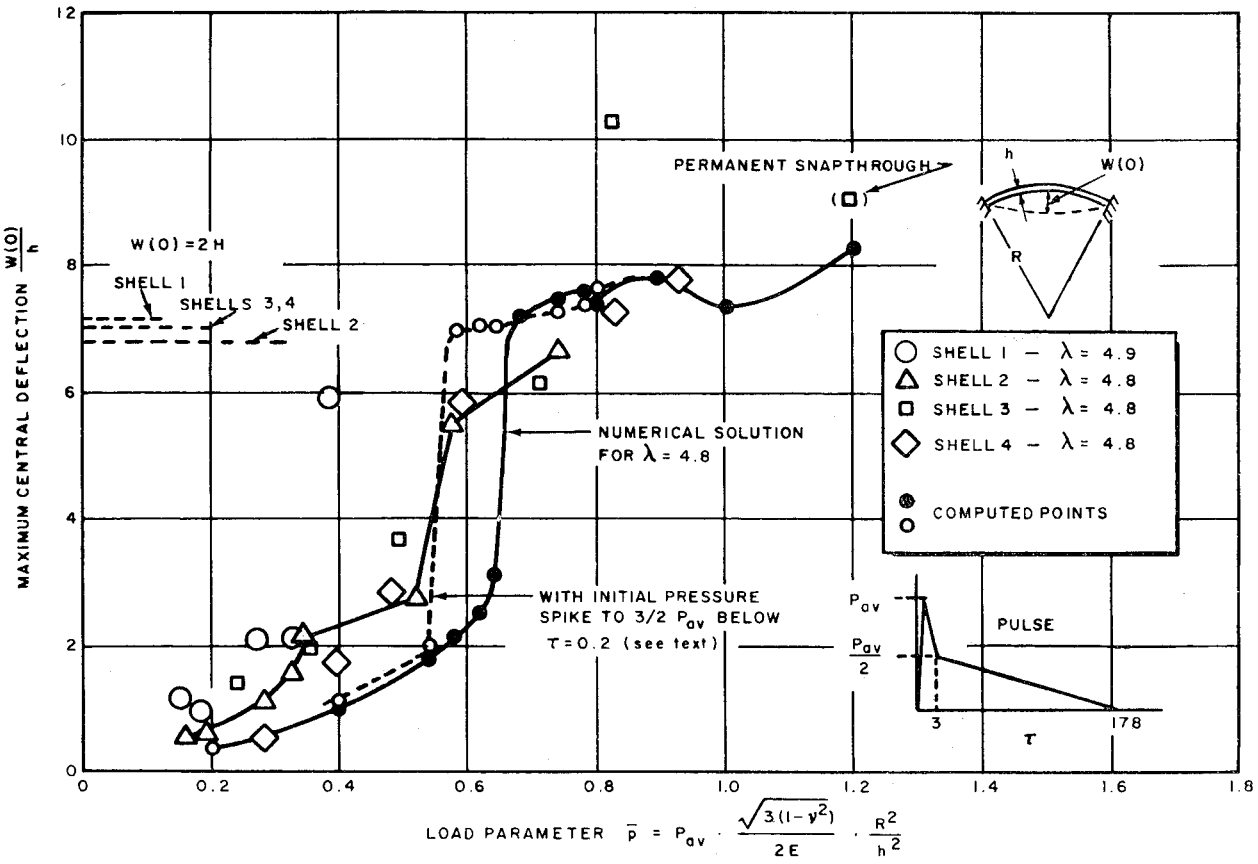

Fig. 8 Test results compared to theory for maximum deflection.

In these definitions, E is Young's modulus, ν is Poisson's ratio, and ρ is the material density. The reference pressure q_0 is the classical, small-deflection-theory buckling pressure of a complete spherical shell.

Values of the coefficients a_n are then computed, along with an "average deflection" quantity $W_{av}/(Z_0)_{av}$. The pressure parameter is given to the machine as any stepwise linear function of τ. In the present case, the recorded pressure-time history of the blast wave on the shell (see, for example, Fig. 5) was approximated and is shown together with its nondimensional counterpart in Fig. 10. A finite rise time was necessary here because of the particular nature of the numerical solution procedure, even though, as mentioned previously, the actual rise time is essentially negligible. The rise time consisted of the smallest basic time interval used in the finite difference computation. The effect of including such a fictitious rise time is to miss a small amount of the impulse that has actually been applied to the shell (for the same peak pressure and decay times). This will be significant in determining response maxima only for cases where the peak pressure is near the critical buckling level. The net effect will be to displace the "critical" region of the response curve of Fig. 8 slightly toward higher values of p. This partially accounts for the observed difference between experimental and computer results.

The computer program was run at $\lambda = 4.8$ (corresponding to the measured value for the models) for various values of $\bar{p}$ ranging from 0.2 and 1.2, in which the decay times remained fixed and only the magnitude of the pressure changed. These pressures covered the range of peak pressures found during the testing. For each peak pressure $\bar{p}$ (note that the entire pressure-time history is known, once $\bar{p}$ is given), the maximum, nondimensional center deflection was computed. It is plotted in Fig. 8 for direct comparison with the central deflection pickup results.

The shell specimens described previously were designed to have a geometric parameter λ of 5 although two different sets of the geometric quantities R, h, and H were used to achieve this. For the first two models, $R = 72$ in., whereas for the last two, $R = 89$ in. This means that the dimensionless time τ will vary at any real time t between the two sizes of model, and that, in precise terms, the pulse-decay times τ_1 and τ_2 should vary in the two cases, so that the real-time pulse remains the same. It was decided, however, that the variation in predicted maximum deflection caused by this difference would be small, especially when set against the uncertainties introduced by errors in some of the measured quantities (in particular R itself). Thus, the values chosen for decay times ($\tau_1 = 3$, $\tau_2 = 178$) would represent a case between the two actual shell sizes, which is expected to apply equally well to both, within the limits of experimental error.

The possible effect on response of an initial very short-time spike, which as previously mentioned may be cut off by slow response (in the μsec range) of the pressure pickup and associated circuitry, was also considered in an extreme case in the numerical computations. A modified pressure pulse (see Fig. 11) rising to $\frac{3}{2}\bar{p}$ at $\tau = 0.1$ decaying back to the previous pulse shape at $\tau = 0.2$ (about 100 μsec) was used as program input. The results calculated for maximum central deflection are shown in Fig. 8 by a dashed line. It is evident that this added impulse would produce a marked downward shift in the theoretical load level at which a jump in response occurs, but it is unlikely (based on the theoretical shock reflection calculation given previously) that such a spike actually exists to this degree. Away from the buckling level, the change caused by such a spike is small.

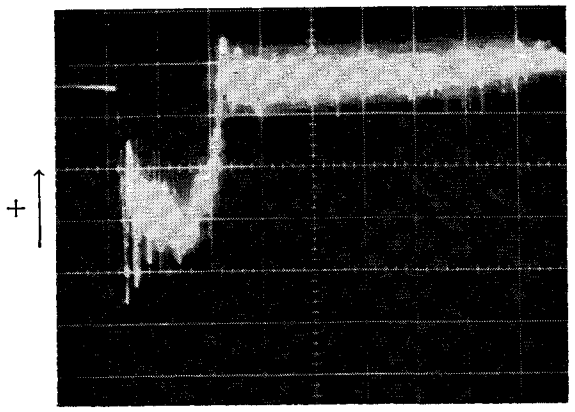

a) Gage 1: Gain 705 μ in./in./cm and Sweep 10 msec/cm

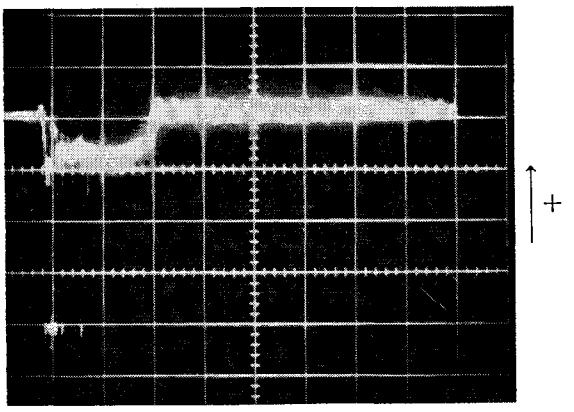

b) Gage 7: Gain 2010 μ in./in./cm and Sweep 10 msec/cm

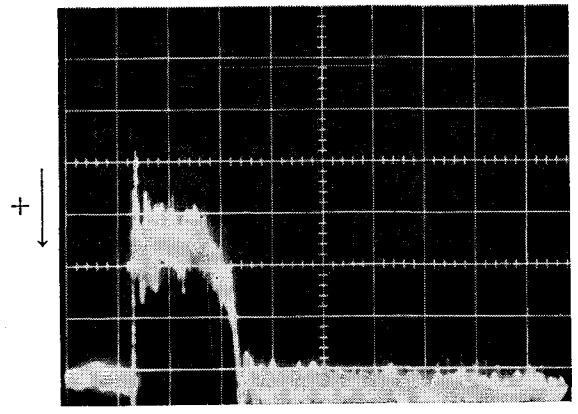

c) Gage 9: Gain 728 μ in./in./cm and Sweep 10 msec/cm

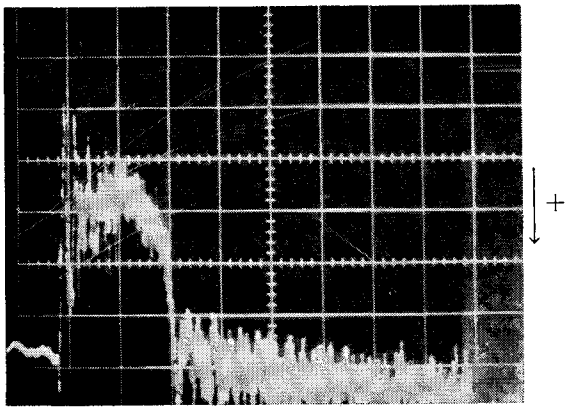

d) Gage 15: Gain 324 μ in./in./cm and Sweep 10 msec/cm

Fig. 9 Sample radial strains; test 192-12-90° apart on circle r = 7.5 in:

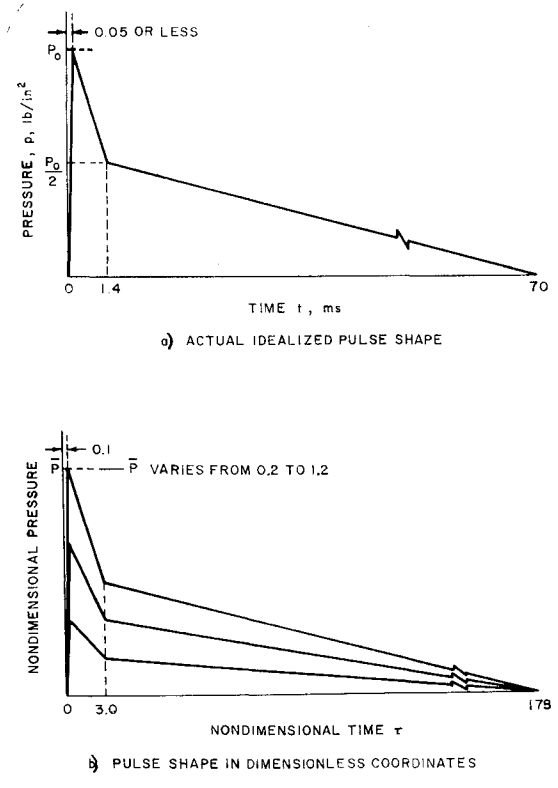

Fig. 10 Pressure pulse used in computations.

VI. Comparisons and Conclusions

In general, the comparison in Fig. 8 shows, as may be expected, that the jump in maximum response, which can be called "dynamic buckling," occurs experimentally at slightly lower peak pressures than predicted. This is in accord with almost all previous reported experimental buckling work and gives an indication of the degree to which the theoretical idealizations of perfect shape and symmetrical deformations are not fulfilled. The general shape of the peak response curve of Fig. 8 appears to be more or less verified by the experiments, as suggested on the figure, although a considerable degree of scatter is present. A fixed amount of uncertainty ($\Delta W/h$ = 0.25) is introduced by the displacement gage because of the stepwise nature of its information. The indirect means of empirically measuring the radius R (inferred from the cap height H) allows for considerable variation, possibly $\pm$ 10%, in the parameter $\bar{p}$, which depends on R^2. Uncertainties in the pressure calibration must also be added in, and the combination of these effects will account for most of the scatter.

It is of interest that the numerical solution for the change with peak pressure of peak deflection W at the center shows a somewhat less steep jump at "buckling" levels than does the average response $\Delta = W_{av}/Z_{0\,av}$ (see Fig. 12). If overall instability is of concern, this average deflection Δ may be a better indication of it than is the central deflection (or the deflection at any single point). On the other hand, the maximum deflection certainly occurs at the center, and this parameter may be of primary importance from the damage point of view.

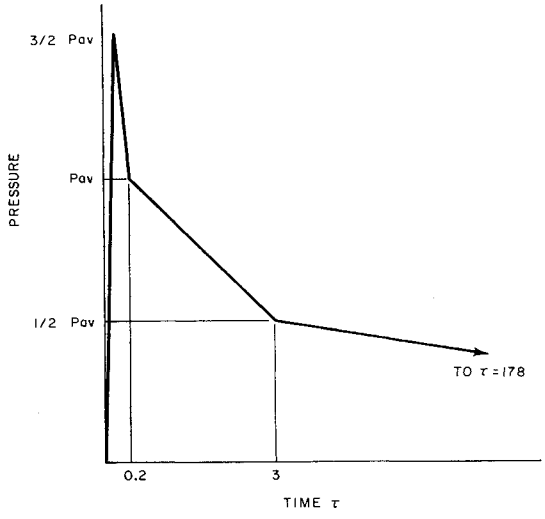

Fig. 11 Modified pressure pulse.

It is seen then, as a general conclusion, that the five-mode, symmetric dynamic buckling theory of Budiansky and Roth[1] gives somewhat unconservative predictions of maximum deflections or critical buckling pressures for a shallow spherical cap under blast loading. It appears that maximum deflections are underestimated at prebuckling levels by as much as 100% (although very close for postbuckling loads), whereas critical buckling pressure is overestimated by 10 to 20%. This is in keeping with the Budiansky-Roth observation[1] that the theory would be expected to be better as a predictor of average results such as buckling than of detailed response at a particular point.

Another aspect of the present test series from the design viewpoint which deserves mention is that deep spherical

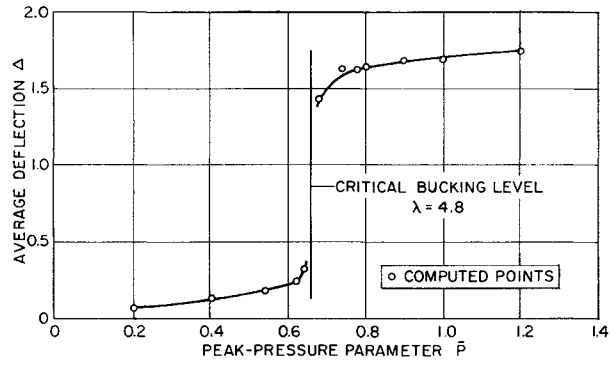

Fig. 12 Computed maximum average deflection for pulse shape used.

shells, as long as they are thin, show a definite tendency to buckle initially (under static load) in a small dimple, which then spreads to include the whole shell (see for example, Homewood, Brine, and Johnson[3]). This dimpled area corresponds in angular extent to the sort of range of shallowness covered in the present tests, and it is likely that these results will give a means of estimating pressure levels for initial instability of deeper spherical caps as well.

References

[1] Budiansky, B. and Roth, R., "Axisymmetric dynamic buckling of clamped shallow spherical shells," NASA TN D-1510, pp. 597–600 (1962).

[2] Courant, R. and Friederichs, K., *Supersonic Flow and Shock Waves* (Interscience Publishers, Inc., New York, 1948), Chap. III, pp. 137–138, 153.

[3] Homewood, R. H., Brine, A., and Johnson, A. E., Jr., "Buckling instability of monocoque shells," Proc. Soc. Exptl. Stress Anal. **18**, 88–96 (1961).